Supplementary Information (SI) for Physical Chemistry Chemical Physics.
This journal is © the Owner Societies 2025

Supplementary Information

Thermally Activated Delayed Fluorescence in Aminoacene Linked Phenanthrolines

P. E Swathi Krishna, [a] Hanock Baiju [a] and Mahesh Hariharan*[a]

[a] School of Chemistry, Indian Institute of Science Education and Research Thiruvananthapuram (IISER-TVM),
Maruthamala P.O., Vithura, Thiruvananthapuram, Kerala, 695551, India

Section A: Materials and Methods

All reactions were carried out in oven-dried glassware and wherever necessary, were performed under dry nitrogen in dried, anhydrous solvents using gastight syringes, cannula, and septa. Solvents were dried and distilled by standard laboratory techniques. TLC analyses were performed on recoated aluminum plates of silica gel 60 F254 plates (0.25mm, Merck) and developed TLC plates were visualized under shot and long-wavelength UV lamps. Flash column chromatography was performed using silica gel of 200-400 mesh employing a solvent polarity correlated with the TLC mobility observed for the substance of interest. ^{1}H NMR spectra were measured on a 500 MHz Bruker Avance DPX spectrometer. The internal standard used for ^{1}H NMR is tetramethyl silane (TMS). Mass spectra were obtained using a Bruker UltrafleXtreme MALDI-TOF/TOF with Matrix Assisted Laser Desorption/Ionization (MALDI). Absorption spectra and emission spectra were recorded on Shimadzu UV-3600 UV-VIS-NIR and Horiba Jobin Yvon Fluorolog spectrometers, respectively. The crystals are packed in between quartz plates for the measurements.

1.1 X-ray Crystallography: Good-quality single crystals of appropriate dimensions were used for the X-ray diffraction experiments. Single crystals were mounted using oil (Infineum V8512) on a glass fibre. All measurements were made on a CCD area detector with graphite monochromated Mo Kα radiation. The data was collected using Bruker APEXII detector and processed using APEX2 from Bruker. All structures were solved by direct methods and expanded using Fourier techniques. The non-hydrogen atoms were refined anisotropically. Hydrogen atoms were included in idealized positions, but not refined. Their positions were constrained relative to their parent atom using the appropriate HFIX command in SHELX-97. All programs used during the crystal structure analysis are incorporated in the WINGX software. The full validation of CIFs and structure factors of the BP and NP crystals were performed using the check CIF utility. NP crystals exhibited few alerts in the CIF file. Three-dimensional structure visualization and exploring the crystal packing of the crystals under study were carried out using Mercury 2021.2.0.

1.2 Computational Methods: All ground state geometry optimizations for BP and NP were carried out in Gaussian 16[1] employing the CAM-B3LYP functional and 6-31G(d,p) basis set at the DFT level of theory in vacuum. Vertical excitation energies and oscillator strengths between the electronic states were calculated employing time-dependent DFT (TD-DFT) at the CAM-B3LYP functional and 6-31G(d,p) level of theory. To compute long-range Coulombic coupling, an electronic energy transfer (EET) module available in Gaussian 16 was utilized. Natural transition orbital (NTO) isosurfaces for both BP and NP were generated using Multiwfn 3.8.[2] Visualization states were rendered using VMD 1.9.3 software.[3]

1.3 Electrostatic Potential (ESP): Electrostatic potential maps illustrate the distribution of charge over the molecule. Gaussian supports the cube keyword to generate the cubes separately from the formatted checkpoint file using the cubegen utility program.

1.4 Hirshfeld Analysis:[4] Important intermolecular interactions within the crystal structures of BP and NP were identified through Hirshfeld surface analysis using Crystal Explorer17.[5] Hirshfeld surface is a combination electron densities for the molecule and the proximity of its neighbours, thus providing information about intermolecular interactions . The Hirshfeld surface is defined as a set of points in 3D space where the ratio of promolecule and procrystal electron densities equals 0.5. The exploration of intermolecular contacts is provided by mapping normalized contact distances (d_{norm}), which is a function of a closest distance from the point to the nuclei interior (d_i) and exterior (d_e) to the surface as well as on the van der Waals radii (r^{vdw}). 2D fingerprint plots derived from the Hirshfeld surface analyses, by plotting the fraction of points on the surface as the function of d_i and d_e, provide a visual summary of intermolecular contacts within the crystal.

1.5 Symmetry Adapted Perturbation Theory (SAPT):[6] SAPT(0) analysis was utilized to identify the non-covalent interaction energies of different non-covalent dimers of BP and NP. The SAPT module of the psi4 code was employed, with aug-cc-pVDZ basis set. SAPT(0) calculates the interaction energy into its contributing components. The results obtained from the SAPT(0) analysis are a second-order perturbation expansion constituting first-order electrostatic and exchange energy parts, second-order dispersion, induction, and their exchange counterparts as the perturbation terms.

$$E_{int}^{SAPT(0)} = E_{elc}^{(1)} + E_{ex}^{(1)} + E_{ind}^{(2)} + E_{ind-ex}^{(2)} + E_{dis}^{(2)} + E_{dis-ex}^{(2)}$$

1.6 TheoDORE Analysis :[7] The excitations of the different dimers obtained from the crystal structure were analyzed using TheoDORE. We study dimer systems, where each of the monomers is considered as a fragment. The parameters used to investigate the excited state characteristics are participation ratio (PR), mean position (POS) of initial orbital (hole) and final orbital (electron), and charge transfer character (CT). The magnitude of PR relates to the number of fragments participating in the excitation; hence, in our investigation, the PR ranges from 1 to 2. POS provides the mean position of hole and electron for a particular excitation. Charge transfer states and delocalized Frenkel states show POS = 1.5. If the Frenkel state is localized on monomer A, then POS = 1, and if localized on monomer B, POS = 2, for a dimer AB. Finally, CT is related to the total weight of configurations where initial and final orbitals are situated on different fragments. A CT value of 1 denotes the presence of a charge-separated state, and CT = 0 refers to Frenkel states.

1.7 Non-Covalent Interaction: [8] NCI analysis employs an index based on electron density and its derivatives to identify noncovalent interactions. A two-dimensional plot of reduced electron density (s) against electron density (ρ) and the critical points are associated with the troughs appearing in the plot. Reduced electron density is given by:

$$s = \frac{1}{2(3\pi^2)^{\frac{1}{3}}} \frac{|\nabla \rho|}{\rho^{\frac{4}{3}}}$$

Noncovalent interactions occur in the real space points where these troughs appear. The sign of second derivative of $\rho(\nabla^2\rho)$ is analyzed to distinguish attractive and repulsive interactions. The noncovalent interaction regions are represented in the plot as discs with color ranging from blue (attractive) to red (repulsive) as in the VIBGYOR spectrum.

1.8 Photophysical Measurements: Shimadzu UV-3600 UV-VIS-NIR spectrometer is used for recording absorption spectra and Horiba Jobin Yvon Fluorolog spectrometer for emission measurements respectively. Gated emissions are also performed in Horiba Jobin Yvon Fluorolog spectrometer with IRF greater than 50 µs. In solution, measurements were conducted in toluene, while in the solid state, finely ground powders were used to minimize the influence of crystal packing effects. Additionally, to explore the photophysical behavior in a dispersed, non-crystalline matrix, the molecules were embedded in PMMA and drop-cast onto coverslips.

Section B: Synthesis and Characterization

Scheme 1

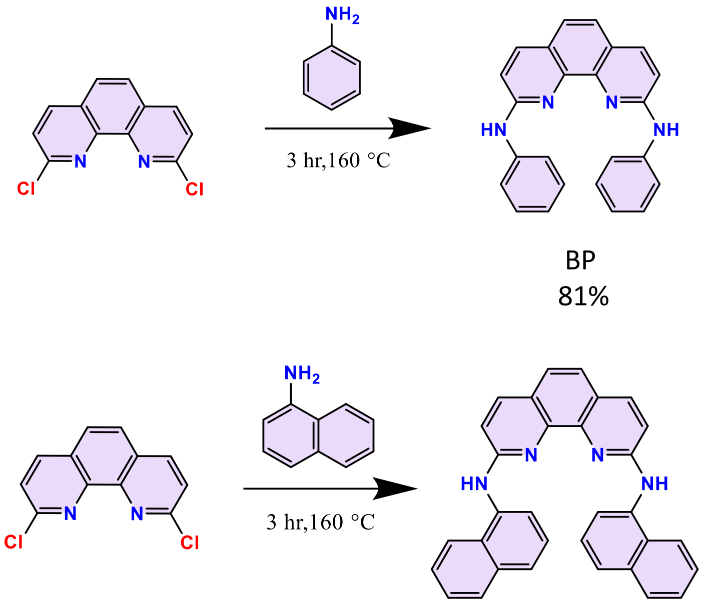

BP
81%

NP
55%

Synthesis of 2,9-Bis(phenylamino)-1,10-phenanthroline

In a 25 ml round bottom flask, a mixture of 2,9-dichloro-1,10-phenanthroline (385 mg, 1.55 mmol) and aniline (3.0 mL) was heated at 160 °C for 2 hrs. The resulting mixture was cooled to 0 °C and saturated aqueous $NaHCO_3$ (20 mL) was added. The mixture was extracted twice with 20 mL of ethyl acetate, dried over anhydrous sodium sulfate, and the organic layer was concentrated under reduced pressure. The residue was purified by column chromatography on silica gel (eluent: ethyl acetate/hexane = 1/3) to yield 2,9-bis(diphenylamino)-1,10- phenanthroline (454 mg, 81%) as a yellow solid; ^{1}H NMR (500 MHz, CDCl3, δ): 8.00 (d, J = 8.8 Hz, 2H), 7.45 (s, 2H), 7.40 (m, 8H), 7.29 (d, J = 8.8 Hz, 2H), 7.13 (t, J = 7.2, 7.2 Hz, 2H); ^{13}C NMR (75.6 MHz, CDCl3, δ): 155.0 (C×2),144.4 (C×2), 140.4 (C×2), 138.1 (CH×2), 129.5 (CH×4), 124.2 (C×2), 123.4 (CH×2), 122.4 (CH×2), 121.3 (CH×4), 110.7 (CH×2); MALDI TOF m/z: [M]+ calcd for $C_{24}H_{19}N_4$: 362.1504, found 362.5504.

Synthesis of 2,9-bis(1-naphtylamino)-1,10-phenanthroline

In a 25 ml round bottom flask, a mixture of 2,9-dichloro-1,10-phenanthroline (312 mg, 1.25 mmol) and 1-naphthylamine (1.794 g, 12.5 mmol) was heated at 160 °C for 2 hrs. The mixture was extracted twice with 20 mL of ethyl acetate, dried over anhydrous sodium sulfate, and the organic layer was concentrated under reduced pressure. The resulting residue was purified by column chromatography on silica gel (eluent: ethyl acetate/hexane = 1/4) to yield 2,9-bis(1-naphthylamino)-1,10-

phenanthroline (318 mg, 55%) as a yellow solid; ^{1}H NMR (500 MHz, CDCl3, δ): 8.20 (2H, d, J = 8.2 Hz), 7.93 (4H, d, J = 8.8 Hz), 7.79 (2H, d, J = 8.2 Hz), 7.50 (8H, m), 7.45 (2H, s), 6.97 (2H, d, J = 9.2 Hz); ^{13}C NMR (125.8 MHz, CDCl3, δ): 155.7 (C×2), 143.1 (C×2), 137.2 (CH×2), 135.0 (C×2), 133.7 (C×2), 128.8 (C×2), 127.4 (CH×2), 125.4 (CH×2), 125.4 (CH×2), 124.9 (CH×2), 124.9 (CH×2), 123.1 (C×2), 121.7 (CH×2), 121.3 (CH×2), 120.1 (CH×2), 109.7 (CH×2): MALDI TOF m/z: [M]+ calcd for $C_{32}H_{23}N_4$: 462.1818, found 462.4517.

Characterization

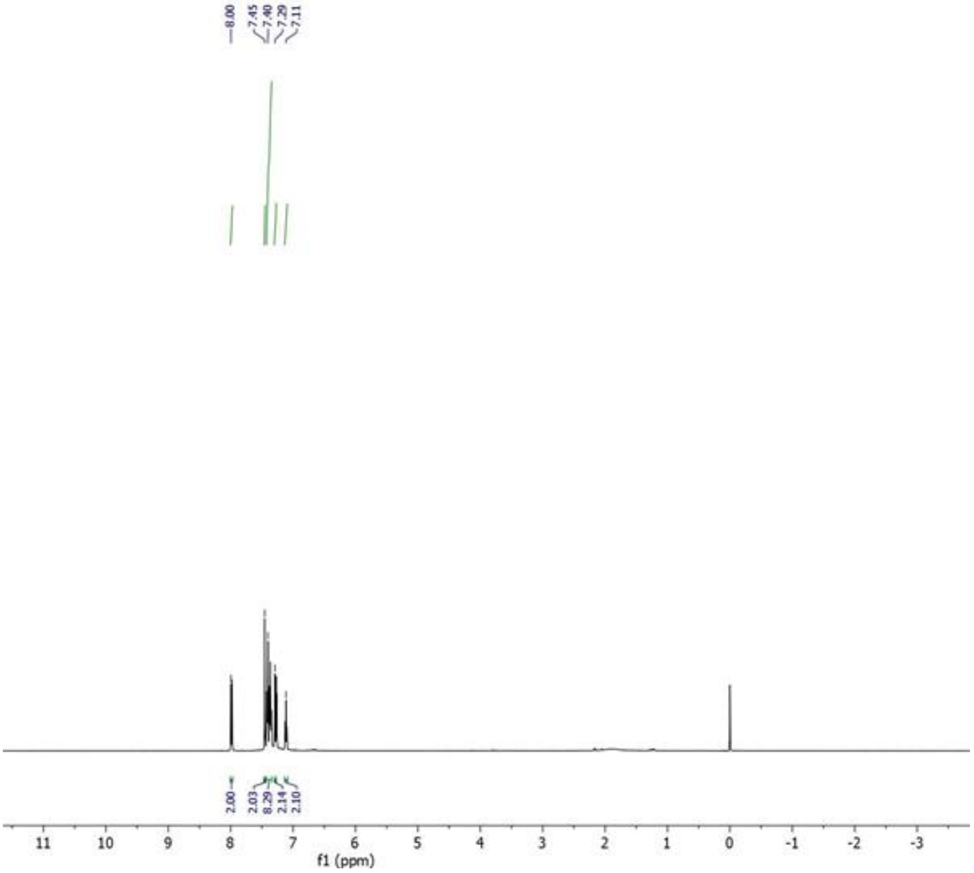

^{1}H NMR spectrum of BP in $CDCl_3$.

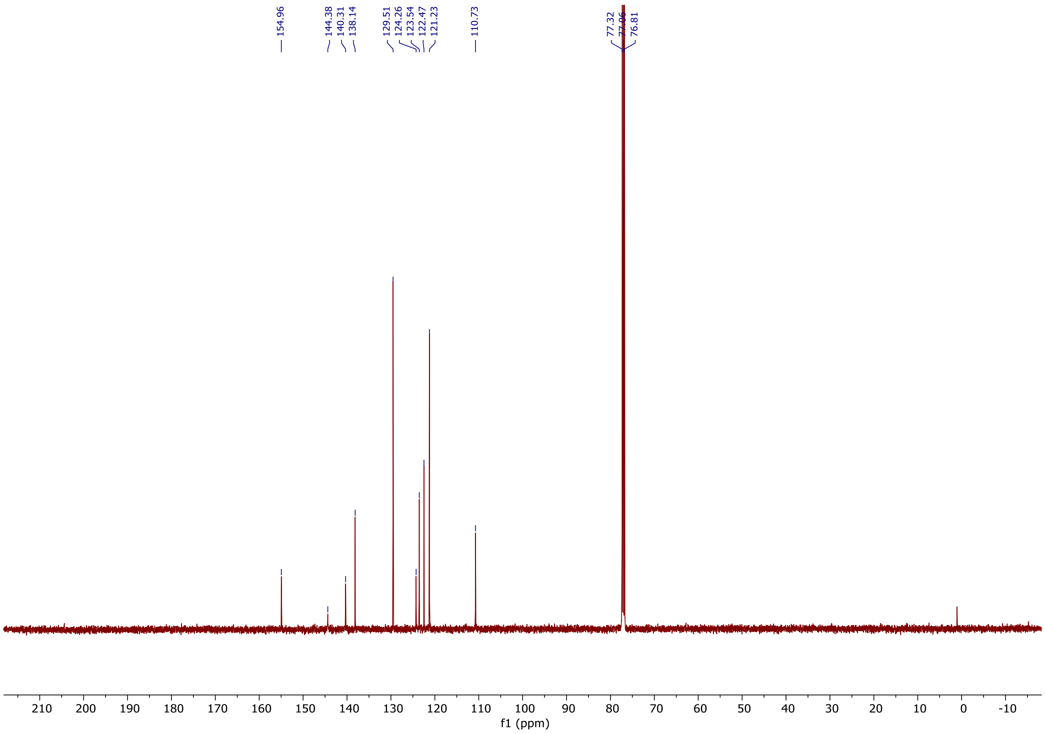

^{13}C NMR spectrum of BP in $CDCl_3$.

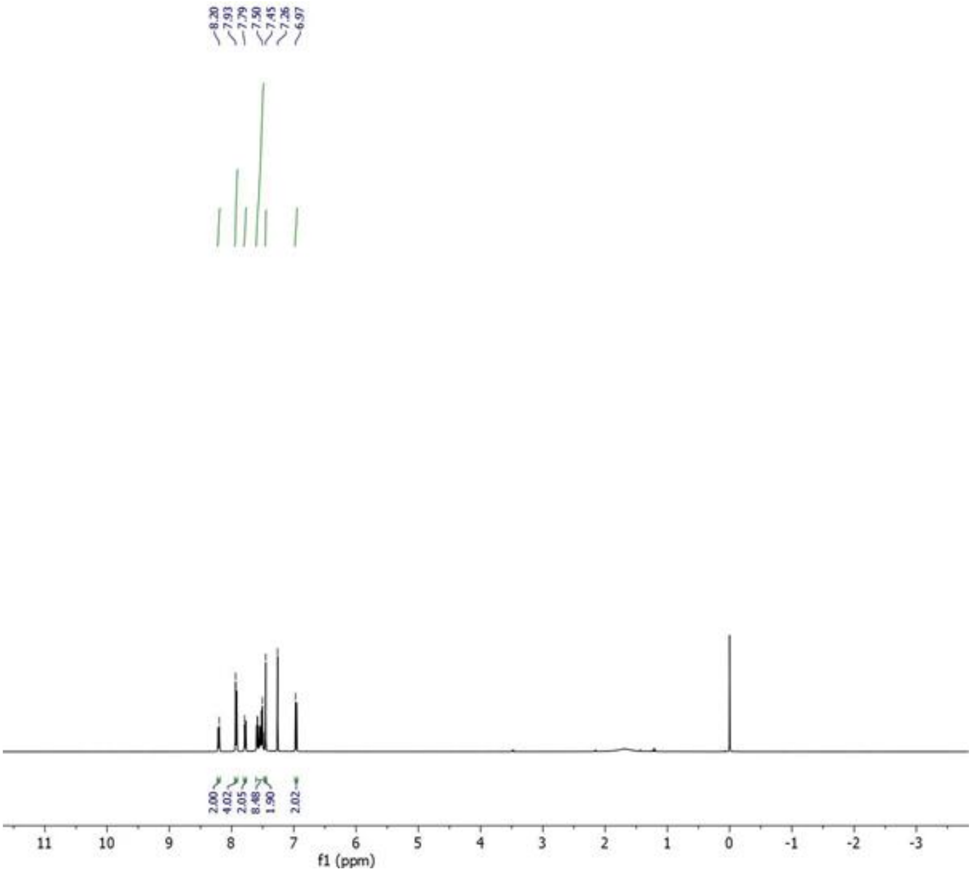

^{1}H NMR spectrum of NP in $CDCl_3$.

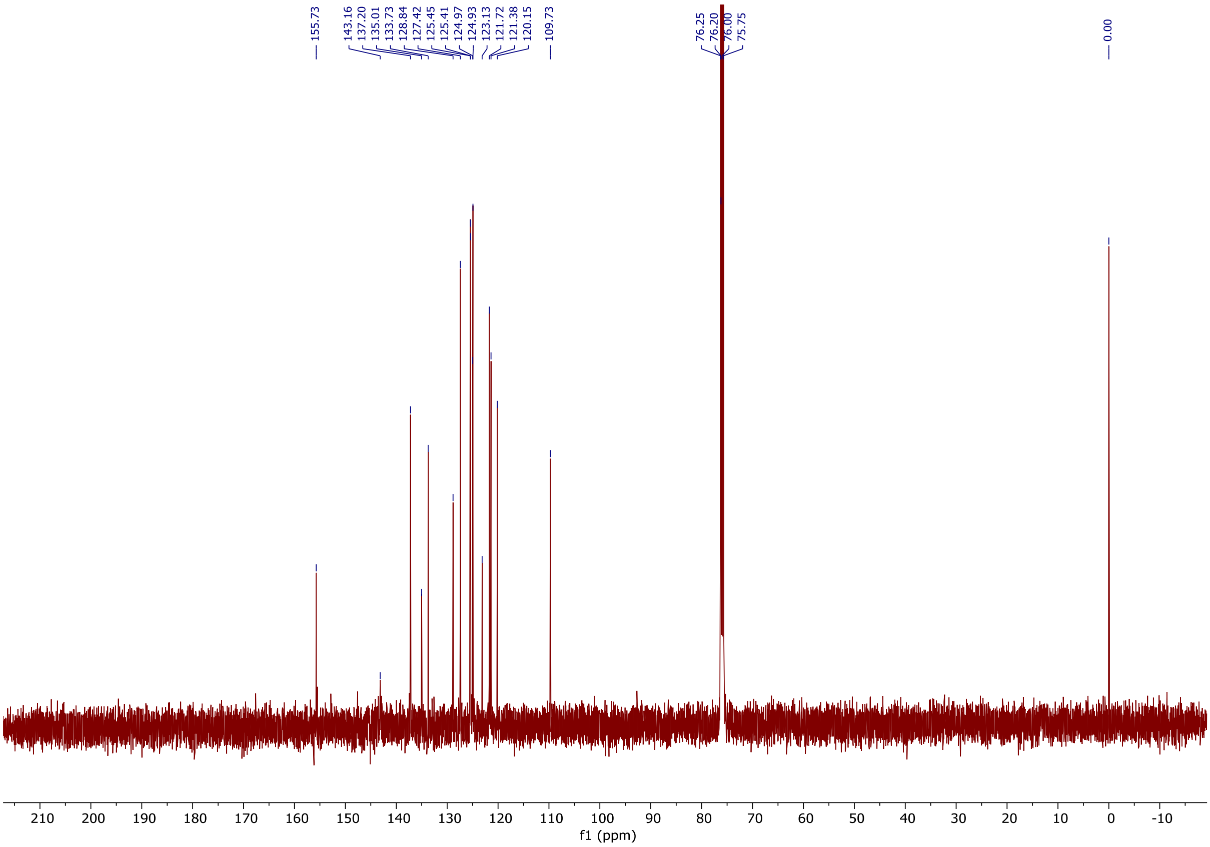

^{13}C NMR spectrum of NP in $CDCl_3$.

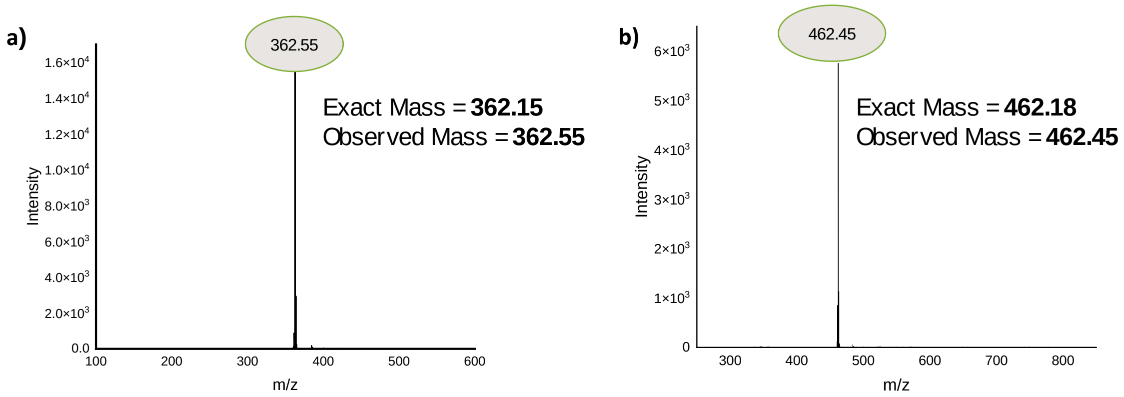

MALDI mass spectrum of a) BP and b) NP with the highlighted molecular mass

Section C: Tables

Table S1. Crystallographic data of BP and NP.

Parameters	BP	NP
Formula	$C_{24}H_{18}N_4$	$C_{96}H_{70}N_{12}O_2$
Formula Weight	362.42	1423.64
Crystal System	Monoclinic	Monoclinic
Space group	P 21/n	C 2/c
a, Å	15.667(3)	21.342(4)

b, Å	10.207(2)	16.508(3)
c, Å	23.640(5)	22.533(5)
α, deg	90	90.00(3)
β, deg	101.832(6)	104.29(3)
γ, deg	90	90.00(3)
Volume, Å^3	3700.1(13)	7693(3)
Z	8	4
Temperature, K	296(2)	296(2)
Density (calculated), mg/m^3	1.301	1.229
R factor (%)	7.2	6.18
Reflections collected	42901	53083
Independent reflections	4510	3261
Goodness of fit	0.994	0.986
CCDC Number	2411806	2411807

Table S2. Percentage of intermolecular interactions present in BP and NP derived from Hirshfeld surface analysis.

Interactions	**BP**	**NP**
H···H	49.80%	58.20%
C···H	37.50%	31.70%
H···N	8.60%	4.40%
C···C	3.00%	3.60%
C···N	1.10%	0.50%
N···N	0.10%	0.20%
H···O	0.00%	1.40%

Table S3. Packing motifs in phenanthroline derivatives.

Entry	**%C···H**	**%C···C**	**ρ=%C···H/%C···C**	**Motif**
BP	37.50	3.00	12.5	Herringbone
NP	31.70	3.60	8.8	Herringbone

Table S4. SAPT(0) analysis of interaction energy components, detailing electrostatic, exchange, induction, and dispersion contributions in BP.

BP	**Electrostatics (kcal/mol)**	**Exchange (kcal/mol)**	**Induction (kcal/mol)**	**Dispersion (kcal/mol)**	**Total SAPT(0) (kcal/mol)**
Dimer 1	-6.99	12.11	-2.05	-19.47	-16.40
Dimer 2	-4.95	8.80	-1.71	-17.10	-14.96
Dimer 3	-0.04	0.47	-0.05	-1.29	-0.91

Dimer 4	-1.09	2.35	-0.28	-4.86	-3.90

Table S5. SAPT(0) analysis of interaction energy components, detailing electrostatic, exchange, induction, and dispersion contributions in NP.

NP	**Electrostatics (kcal/mol)**	**Exchange (kcal/mol)**	**Induction (kcal/mol)**	**Dispersion (kcal/mol)**	**Total SAPT(0) (kcal/mol)**
Dimer 1	-9.04	18.33	-3.49	-33.77	-27.97
Dimer 2	-5.40	11.52	-1.24	-22.58	-17.71
Dimer 3	-2.14	3.16	-0.43	-4.96	-4.37
Dimer 4	0.12	0.75	-0.21	-2.85	-2.19
Dimer 5	-1.41	2.28	-0.35	-4.64	-4.13

Table S6. Coulombic coupling values calculated from the lowest two singlets for all dimers selected for a) BP and b) NP (values are in cm^{-1}).

a)

		S_1	S_2
D1	S_1	205.68	61.76
	S_2	77.98	-85.65
D2	S_1	-0.33	-2.27
	S_2	-2.27	108.34
D3	S_1	58.70	-100.80
	S_2	3.96	98.86
D4	S_1	-29.43	36.07
	S_2	36.07	-186.07
D5	S_1	-3.00	12.85
	S_2	-21.04	-16.48

b)

		S_1	S_2
D1	S_1	-7.51	-21.35
	S_2	24.11	139.64
D2	S_1	-11.30	24.40
	S_2	-82.78	106.27
D3	S_1	0.54	5.37
	S_2	5.34	48.32
D4	S_1	0.83	-5.36
	S_2	-2.78	-69.95

Table S7. TD-DFT analysis showing electronic excitation energies and oscillator strengths for BP monomer.

Singlets	**Energy(eV)**	**Oscillator strength**	**Triplets**	**Energy(eV)**
S_1	3.7164	0.0014	T_1	2.7035
S_2	4.0024	0.3302	T_2	2.9850
S_3	4.1855	0.0738	T_3	3.2398
S_4	4.7220	0.9011	T_4	3.3417
S_5	4.7854	0.0004	T_5	3.5593
S_6	4.8715	0.0008	T_6	3.8921
S_7	4.8852	0.0001	T_7	4.0999
S_8	4.9263	0.0193	T_8	4.1693
S_9	4.9617	0.1003	T_9	4.2046

S_{10}	5.0382	0.3161	T_{10}	4.3093

Table S8. TD-DFT analysis showing electronic excitation energies and oscillator strengths for NP monomer.

Singlets	**Energy(eV)**	**Oscillator strength**	**Triplets**	**Energy(eV)**
S_1	3.7404	0.0023	T_1	2.4167
S_2	3.8233	0.9296	T_2	2.4504
S_3	4.0500	0.2618	T_3	2.7312
S_4	4.2844	0.2385	T_4	3.0077
S_5	4.4331	0.0229	T_5	3.3999
S_6	4.4651	0.0221	T_6	3.6183
S_7	4.4845	0.0363	T_7	3.8470
S_8	4.8434	0.0005	T_8	3.9240
S_9	4.8824	0.0900	T_9	3.9666
S_{10}	5.0474	0.1824	T_{10}	4.0178

Table S9. Temperature-dependent lifetime data of BP.

Temperature	τ_{DF}	τ_{P}
77 K	within the pulse width	909.0 µs

157 K	within the pulse width	109.2 µs, 1.25 ms
207 K	within the pulse width	77.4 µs, 575.0 µs
257 K	153.5 µs	454.0 µs

Table S10. Temperature-dependent lifetime data of NP.

Temperature	**τ_{DF} (µs)**
77 K	91.4
157 K	160.3
207 K	362.1
257 K	387.5
297 K	395.4

Table S11. Fragment based excited state analysis for BP.

Energy state	dE(eV)	f	POS	PR	CT
S_1	3.716	0.001	1.206	1.48	0.386
S_2	4.002	0.33	1.378	1.711	0.537
S_3	4.186	0.074	1.267	1.536	0.506
S_4	4.722	0.901	1.421	1.632	0.597
S_5	4.785	0	1.065	1.141	0.124
S_6	4.872	0.001	1.532	1.965	0.51
S_7	4.885	0	1.532	1.952	0.506

S_8	4.926	0.019	1.793	1.49	0.339
S_9	4.962	0.1	1.791	1.493	0.286
S_{10}	5.038	0.316	1.434	1.879	0.515

Table S12. Fragment based excited state analysis for NP.

Energy state	dE(eV)	f	POS	PR	CT
S_1	3.74	0.002	1.205	1.48	0.373
S_2	3.823	0.93	1.568	1.962	0.371
S_3	4.05	0.262	1.772	1.541	0.364
S_4	4.284	0.238	1.288	1.588	0.493
S_5	4.433	0.023	1.561	1.965	0.271
S_6	4.465	0.022	1.944	1.965	0.11
S_7	4.843	0.001	1.04	1.965	0.078
S_8	4.882	0.09	1.418	1.965	0.518
S_9	5.047	0.182	1.593	1.965	0.335
S_{10}	5.108	0.001	1.65	1.965	0.467

Table S13 The dipole moments of BP and NP calculated at cam-b3lyp/6-31+g(d,p) level of theory in three dielectrics, toluene, THF and acetonitrile.

	BP		NP	
	S_0	S_1	S_0	S_1
Toluene	3.5007	3.1017	0.3260	1.2938

THF	3.9126	3.5780	0.6365	1.5799
Acetonitrile	4.1117	3.8121	0.8566	1.8002

Section D: Figures

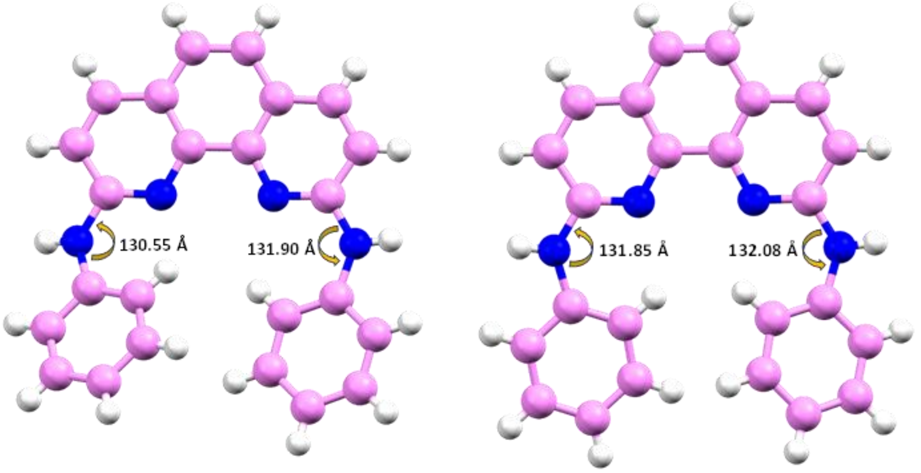

Figure S1. Schematic representation showing the asymmetric units with their corresponding torsional angles in BP.

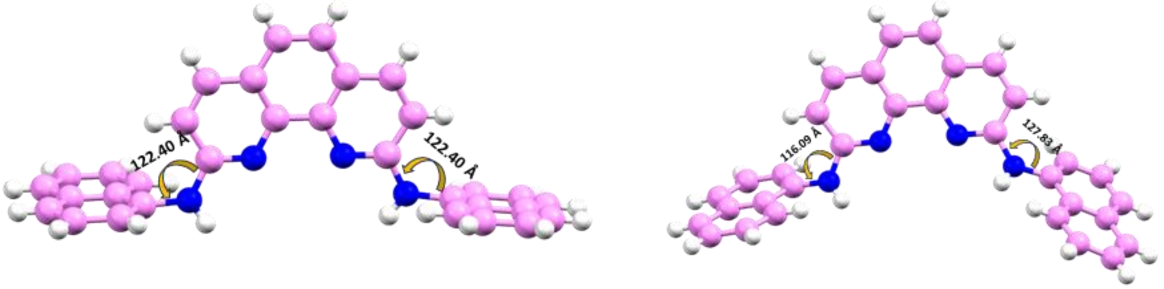

Figure S2. Schematic representation showing the asymmetric units with their corresponding torsional angles in NP.

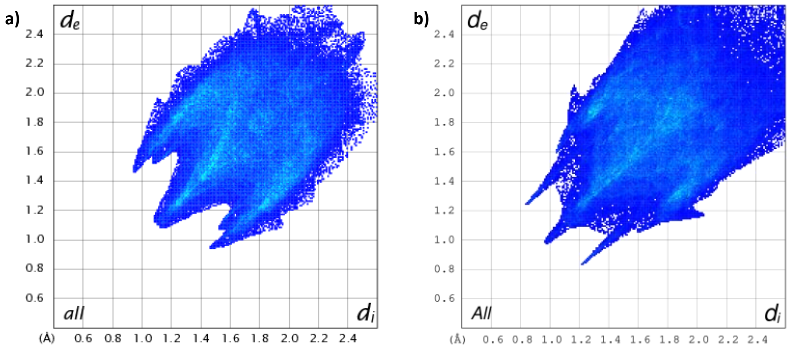

Figure S3. Hirshfeld 2D fingerprint plot of (a) BP and (b) NP.

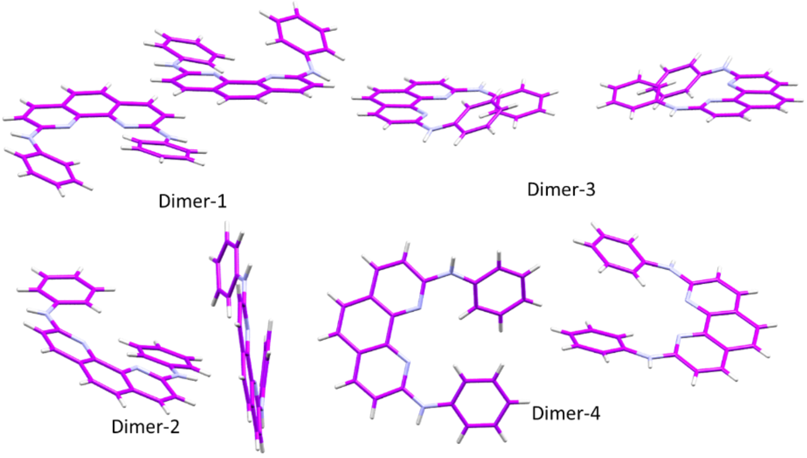

Figure S4. The distinct dimers present in the crystal lattice of BP.

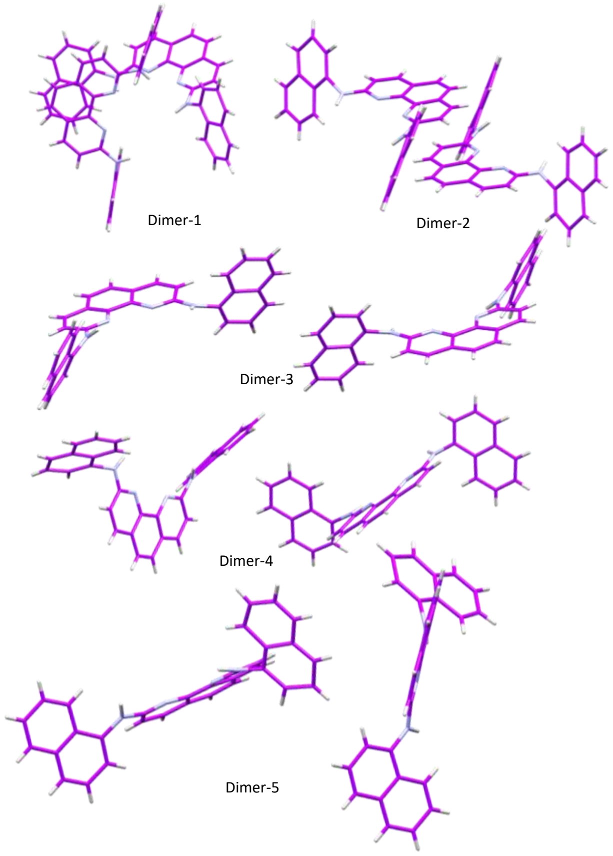

Figure S5. The distinct dimers present in the crystal lattice of NP.

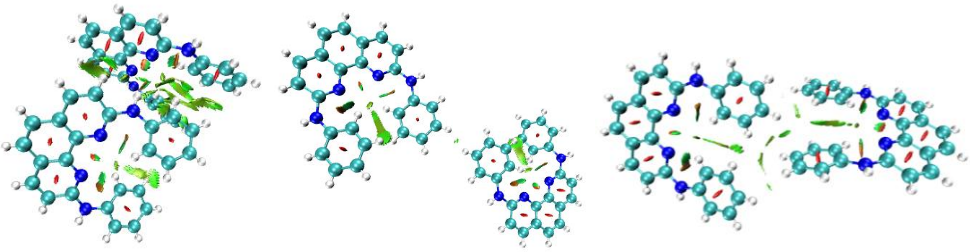

Dimer 2 **Dimer 3** **Dimer 4**

Figure S6. The non-covalent interaction analysis for distinct dimers of BP contributing to crystal packing. Green discs and red discs represent stabilizing and destabilizing interactions, respectively.

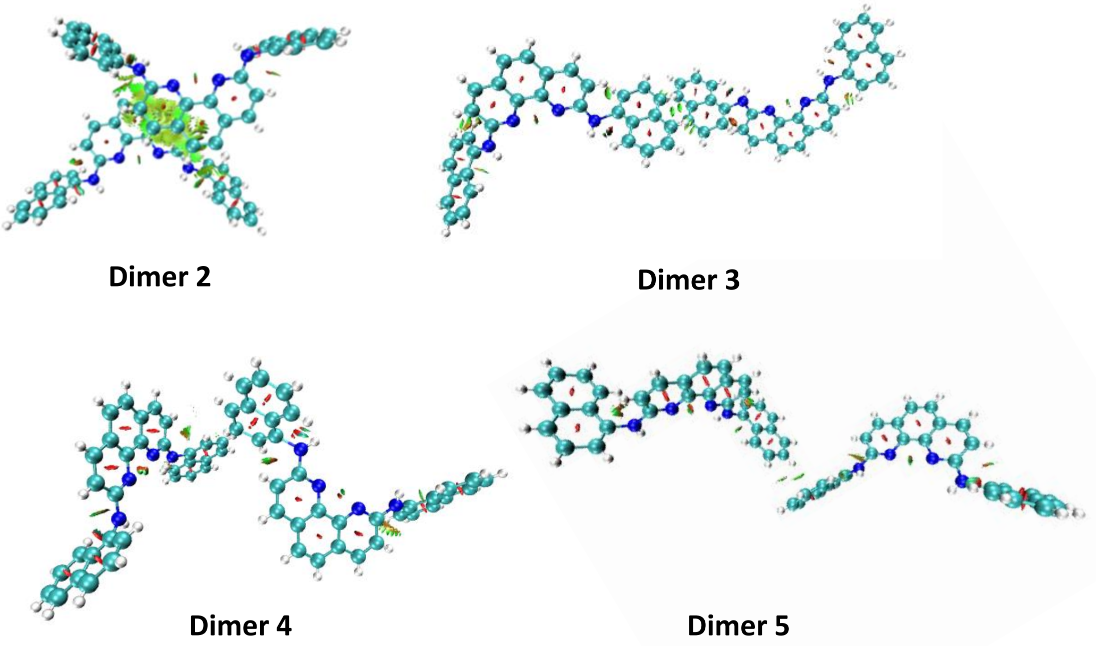

Figure S7. The non-covalent interaction analysis for distinct dimers of NP contributing to crystal packing. Green discs and red discs represent stabilizing and destabilizing interactions, respectively.

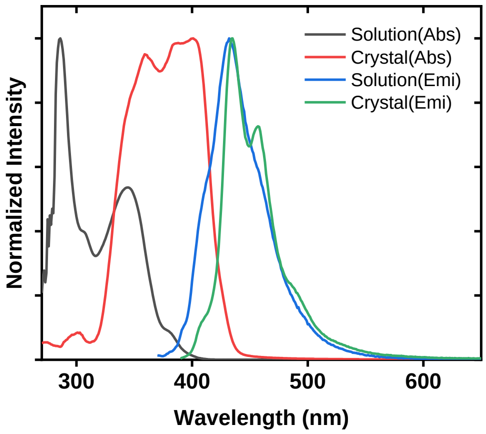

Figure S8. Absorption and emission spectra of BP in crystalline and solution states.

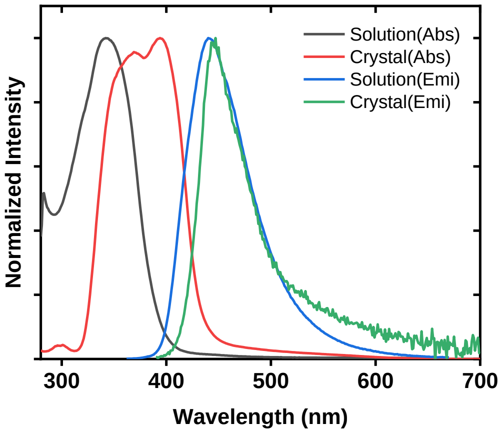

Figure S9. Absorption and emission spectra of NP in crystalline and solution states.

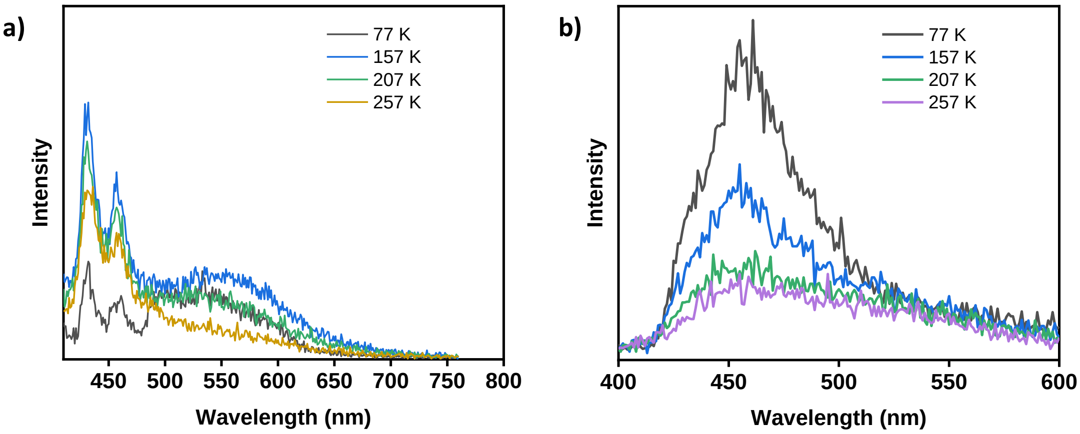

Figure S10. Temperature-dependent delayed emission plots of (a) BP and (b) NP.

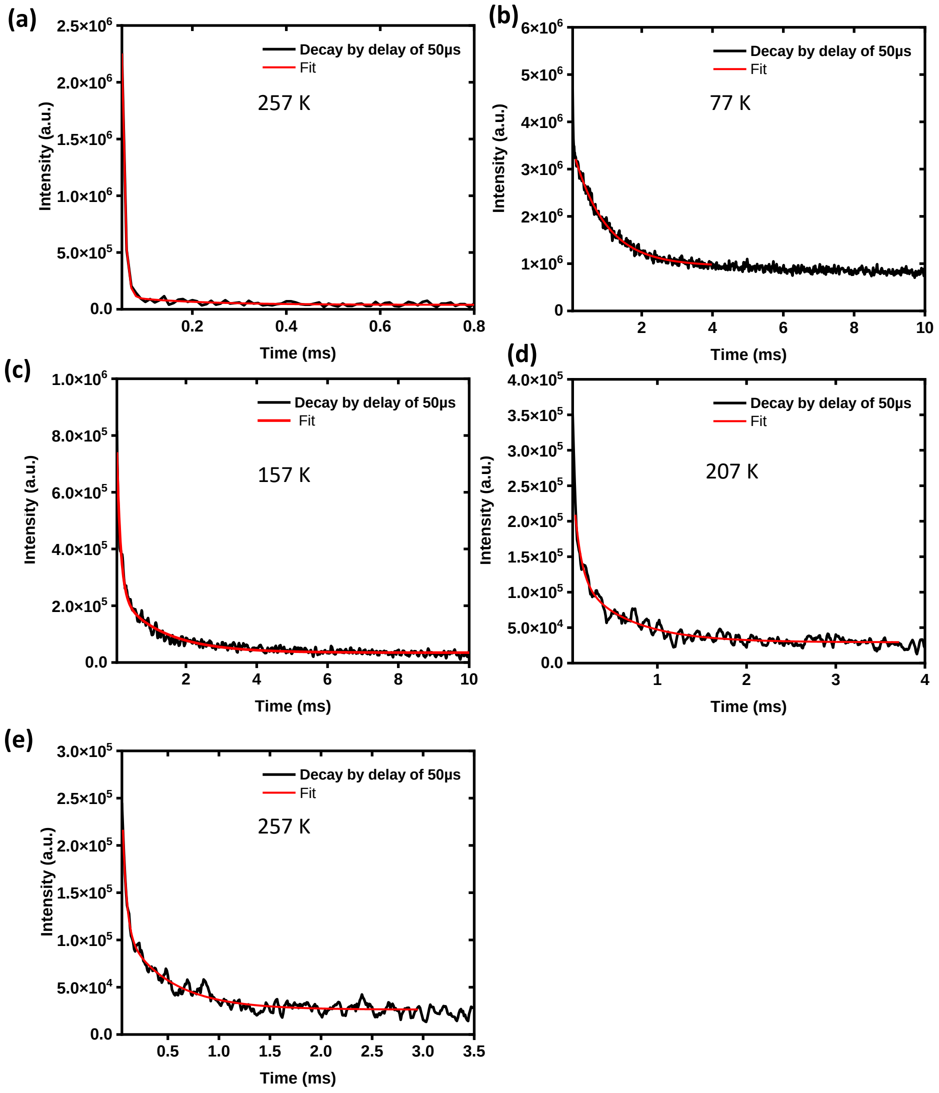

Figure S11. Decay profiles at various temperatures for BP were collected at a) 429 nm and b), c), d), e) at 520 nm.

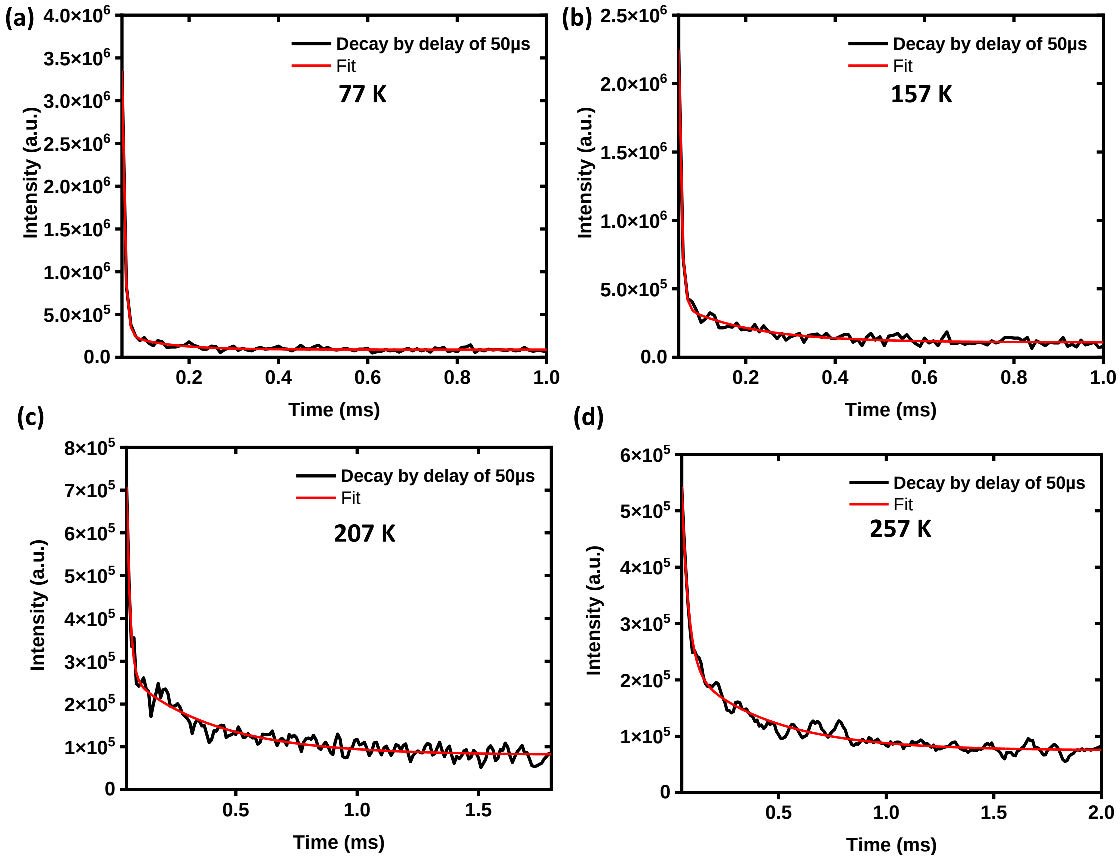

Figure S12. Decay profiles at various temperatures for NP collected at its emission maximum.

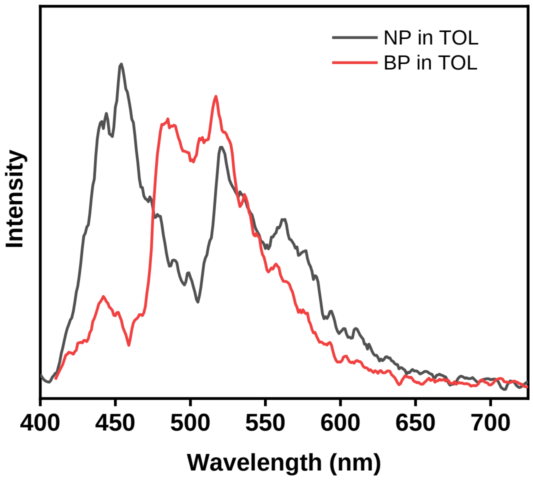

Figure S13. Delayed emission spectra of BP and NP at 77 K (in liquid N_2) in toluene.

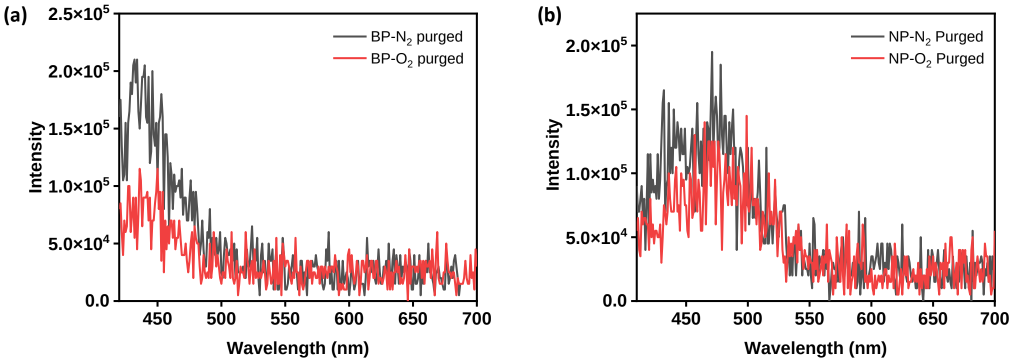

Figure S14. Gated emission spectra of (a) BP and (b) NP in toluene under nitrogen- and oxygen-purged conditions.

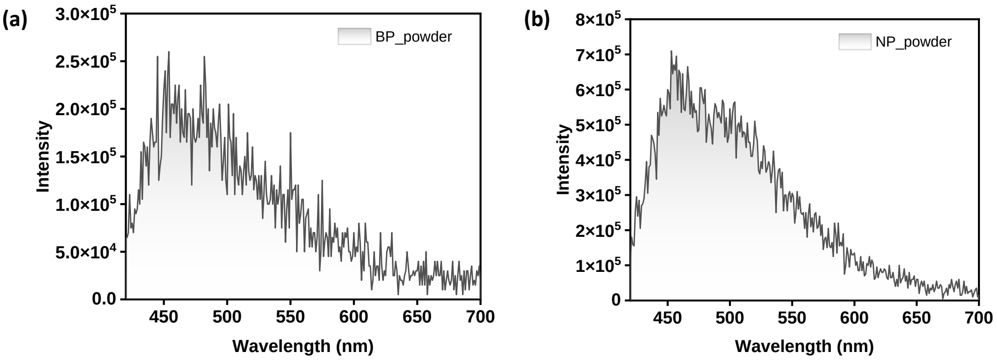

Figure S15. Gated emission spectra of (a) BP and (b) NP in their amorphous forms.

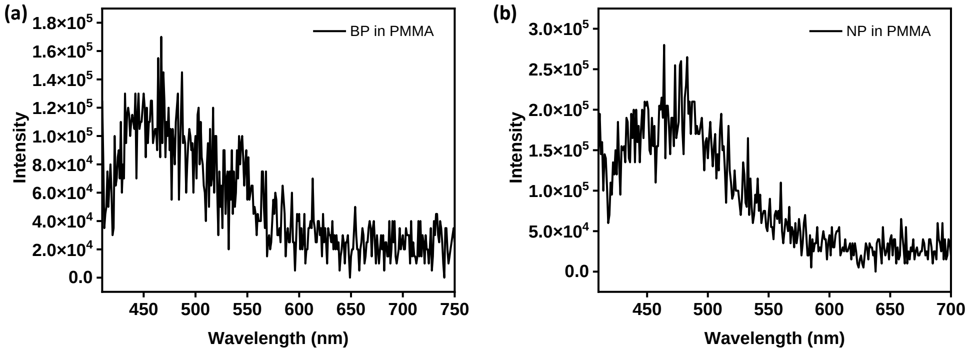

Figure S16. Gated emission spectra of (a) BP and (b) NP embedded in PMMA films drop-cast onto glass coverslips.

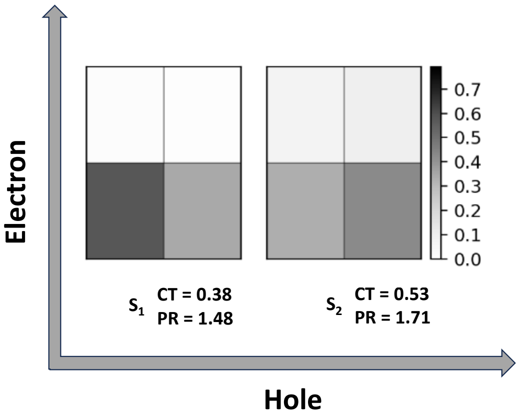

Figure S17. Electron Hole correlation plot of S_1 and S_2 states of BP.

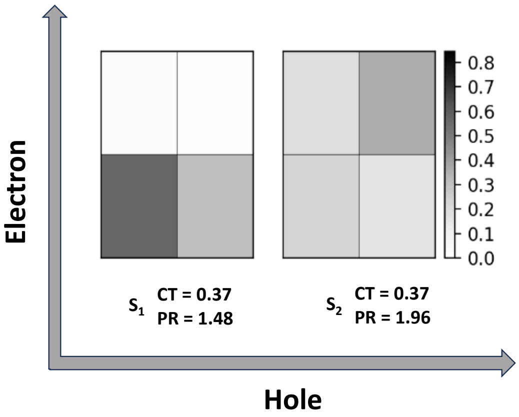

Figure S18. Electron Hole correlation plot of S_1 and S_2 states of NP.

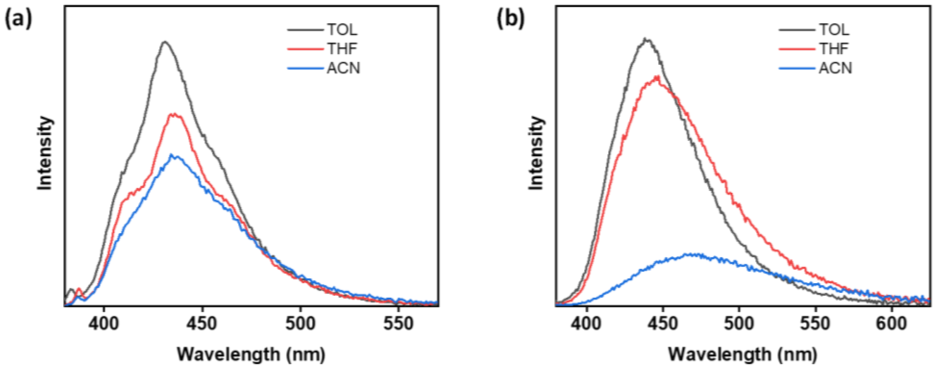

Figure S19. Solvent-dependent emission spectra of (a) BP and (b) NP recorded in toluene (TOL), tetrahydrofuran (THF), and acetonitrile (ACN).

References

[1] M. J. Frisch, G. W. Trucks, H. B. Schlegel, G. E. Scuseria, M. a. Robb, J. R. Cheeseman, G. Scalmani, V. Barone, G. a. Petersson, H. Nakatsuji, X. Li, M. Caricato, a. V. Marenich, J. Bloino, B. G. Janesko, R. Gomperts, B. Mennucci, H. P. Hratchian, J. V. Ortiz, a. F. Izmaylov, J. L. Sonnenberg, Williams, F. Ding, F. Lipparini, F. Egidi, J. Goings, B. Peng, A. Petrone, T. Henderson, D. Ranasinghe, V. G. Zakrzewski, J. Gao, N. Rega, G. Zheng, W. Liang, M. Hada, M. Ehara, K. Toyota, R. Fukuda, J. Hasegawa, M. Ishida, T. Nakajima, Y. Honda, O. Kitao, H. Nakai, T. Vreven, K. Throssell, J. a. Montgomery Jr., J. E. Peralta, F. Ogliaro, M. J. Bearpark, J. J. Heyd, E. N. Brothers, K. N. Kudin, V. N. Staroverov, T. a. Keith, R. Kobayashi, J. Normand, K. Raghavachari, a. P. Rendell, J. C. Burant, S. S. Iyengar, J. Tomasi, M. Cossi, J. M. Millam, M. Klene, C. Adamo, R. Cammi, J. W. Ochterski, R. L. Martin, K. Morokuma, O. Farkas, J. B. Foresman, D. J. Fox, **2016**, Gaussian 16, Revision C.01, Gaussian, Inc., Wallin.

[2] R. L. Martin, *J. Chem. Phys.* **2003**, *118*, 4775–4777.

[3] W. Humphrey, A. Dalke, K. Schulten, *J. Mol. Graph.* **1996**, *14*, 33–38.

[4] M. A. Spackman, D. Jayatilaka, *CrystEngComm* **2009**, *11*, 19–32.

[5] C. F. Mackenzie, P. R. Spackman, D. Jayatilaka, M. A. Spackman, *IUCrJ* **2017**, *4*, 575–587.

[6] K. Szalewicz, *Wiley Interdiscip. Rev. Comput. Mol. Sci.* **2012**, *2*, 254–272.

[7] F. Plasser, *J. Chem. Phys.* **2020**, *152*, 84108.

[8] J. Contreras-García, E. R. Johnson, S. Keinan, R. Chaudret, J. P. Piquemal, D. N. Beratan, W. Yang, *J. Chem. Theory Comput.* **2011**, *7*, 625–632.